

# Planetary Core Formation with Collisional Fragmentation and Atmosphere to Form Gas Giant Planets

Hiroshi Kobayashi<sup>1</sup>, Hidekazu Tanaka<sup>2</sup>, Alexander V. Krivov<sup>1</sup>

<sup>1</sup> *Astrophysical Institute and University Observatory, Friedrich Schiller University, Schillergaesschen 2-3, 07745, Jena, GERMANY*

<sup>2</sup> *Institute of Low Temperature Science, Hokkaido University, Kita-Ku Kita 19 Nishi 8, Sapporo 060-0819, JAPAN*

hkobayas@astro.uni-jena.de

## ABSTRACT

Massive planetary cores ( $\sim 10$  Earth masses) trigger rapid gas accretion to form gas giant planets such as Jupiter and Saturn. We investigate the core growth and the possibilities for cores to reach such a critical core mass. At the late stage, planetary cores grow through collisions with small planetesimals. Collisional fragmentation of planetesimals, which is induced by gravitational interaction with planetary cores, reduces the amount of planetesimals surrounding them, and thus the final core masses. Starting from small planetesimals that the fragmentation rapidly removes, less massive cores are formed. However, planetary cores acquire atmospheres that enlarge their collisional cross section before rapid gas accretion. Once planetary cores exceed about Mars mass, atmospheres significantly accelerate the growth of cores. We show that, taking into account the effects of fragmentation and atmosphere, initially large planetesimals enable formation of sufficiently massive cores. On the other hand, because the growth of cores is slow for large planetesimals, a massive disk is necessary for cores to grow enough within a disk lifetime. If the disk with 100 km-sized initial planetesimals is 10 times as massive as the minimum mass solar nebula, planetary cores can exceed 10 Earth masses in the Jovian planet region ( $> 5$  AU).

*Subject headings:* planet and satellites:formation

## 1. Introduction

Gas giant planets such as Jupiter and Saturn form in gaseous disks. In the core-accretion model, the accretion of planetesimals produces cores of giant planets. Once a core reaches a critical mass  $\sim 10$  Earth masses, it can rapidly accrete gas to form a gas giant planet (Mizuno 1980; Bodenheimer & Pollack 1986; Ikoma et al. 2000). Gas giants must form within the lifetime of gaseous disks ( $\lesssim 10$  Myr).

For km-sized or larger planetesimals, gravitational focusing enhances their collisional cross sections, resulting in a high collision probability for low relative velocities. Relative velocities of large bodies are kept lower than those of small ones due to dynamical friction. A combination of gravita-

tional focusing and dynamical friction brings rapid growth of large bodies, which is referred to as runaway growth (Wetherill & Stewart 1989). Eventually, the runaway growth generates a small population of large bodies called planetary embryos. Planetary embryos keep their orbital separations and hence grow through collisions with surrounding remnant planetesimals more slowly than in the runaway mode (Kokubo & Ida 1998). This regime is called oligarchic growth.

Kobayashi et al. (2010) pointed out that the oligarchic growth halts due to fragmentation of planetesimals. In the oligarchic growth, the relative velocities of planetesimals are controlled by the viscous stirring of embryos and gas drag. As embryos grow, the velocities of remnant planetesimals are increased so greatly that collisions be-

tween planetesimals become destructive. Such collisions eject numerous fragments, which collide with each other to produce further smaller bodies. Planetesimals are therefore ground down through such successive collisions (collision cascade). The random velocities of small bodies are strongly damped by gas drag and thereby the collisional cascade no longer occurs for fragments with radii  $\lesssim 1\text{--}10\text{ m}$ . In the end such fragments drift inward due to gas drag and are lost around embryos. The collisional cascade combined with the loss of fragments reduces the solid surface density and hence final embryo masses. Kobayashi et al. (2010) showed that the final embryo masses are as small as Mars mass for 1-100 km-sized planetesimals in the minimum mass solar nebula (hereafter MMSN; Hayashi 1981). Large planetesimals, which are relatively hard to be broken collisionally, and a massive disk produce massive final embryos. However, collisional fragmentation makes it difficult to form giant planets along the lines of the core-accretion model; starting from 100 km-sized planetesimals, planetary embryos can reach the critical core mass for gas accretion only inside 3-4 AU in a disk that is 10 times more massive than the MMSN model.

The motion of fragments  $\lesssim 1\text{ m}$  is coupled with gas. The drift timescale of such fragments are relatively long. Kenyon & Bromley (2009) proposed that embryos may accrete a large amount of such fragments. However, the strong gas drag in the Stokes regime is dominant for fragments  $\lesssim 100\text{ m}$  and damps the relative velocities to halt collision cascade at 1-10 m as mentioned above. Therefore, only a small amount of coupled bodies are produced and hence they hardly contribute to embryo growth (Kobayashi et al. 2010).

Many authors have investigated embryo growth with  $N$ -body, statistical, and hybrid simulations (Kokubo & Ida 1996, 1998, 2000, 2002; Inaba et al. 1999, 2001, 2003; Weidenschilling et al. 1997; Weidenschilling 2005, 2008; Kenyon & Bromley 2004, 2008; Chambers 2006, 2008; Kobayashi et al. 2010). Although providing most accurate dynamical results,  $N$ -body simulations have difficulty in producing numerous fragments and following their fate. The fragmentation effect on embryo growth has thus not been treated in detail in spite of its importance. Recently, Levison et al. (2010) included fragment production in their  $N$ -body

simulation. However, it is still difficult to treat fragment-fragment collisions. Such successive collisions are essential in the collision cascade (e.g., Kobayashi & Tanaka 2010). Therefore, statistical simulations are a better method to accurately investigate planet formation with fragmentation.

In the statistical simulation, the collisional mass evolution of bodies is calculated within a “particle-in-a-box” approximation. Bodies have horizontal and vertical components of random velocity relative to a circular orbit that are determined by their eccentricities and inclinations, respectively. These velocities are changed by gravitational interactions between the bodies and hence affected by their mass spectrum, while the collision rates between the bodies depend on the velocities. Therefore, the coupled mass and velocity evolution needs to be solved (Wetherill & Stewart 1993). While the statistical method has advantages, its weak point is the inability to track the individual positions of planetesimals. However, progress in planetary dynamic theory (Greenzweig & Lissauer 1992; Ida & Nakazawa 1989; Ohtsuki 1999; Stewart & Ida 2000; Ohtsuki et al. 2002) has helped to overcome this problem. For example, Greenzweig & Lissauer (1992) and Ida & Nakazawa (1989) provided detailed expressions for the probability of collisions between planetesimals orbiting a central star, while Stewart & Ida (2000) and Ohtsuki et al. (2002) derived improved equations for calculating the evolution of random planetesimal velocities caused by gravitational interactions. Finally, it has been shown that the recently developed statistical codes can describe some aspects of the planetary accumulation processes with the same accuracy as  $N$ -body simulations (Inaba et al. 2001; Kobayashi et al. 2010).

Since the timescale of collision cascade strongly affects the final mass of planetary embryos (Kobayashi et al. 2010), fragmentation outcome models are essential for embryo growth. Collisional fragmentation includes several uncertain parameters. Kobayashi & Tanaka (2010) constructed a simple fragmentation model which is consistent with laboratory experiments (Fujiwara et al. 1977; Takagi et al. 1984; Holsapple 1993) and hydrodynamical simulations (Benz & Asphaug 1999) and analytically clarified which parameters are essential. They found that the mass de-

pletion due to collision cascades is sensitive to the total ejecta mass yielded by a single collision, while it is almost independent of the mass of the largest ejecta fragment and the size distribution of ejecta over a realistic parameter region. Furthermore, fragmenting collisions are subdivided into two types, catastrophic disruption and cratering (erosive collision). Although some studies neglected or underestimated the effect of cratering (Dohnanyi 1969; Williams & Wetherill 1994; Wetherill & Stewart 1993; Inaba et al. 2003; Bottke et al. 2005), Kobayashi & Tanaka showed that cratering collisions make a dominant contribution to the collision cascade.

A planetary embryo larger than  $\sim 10^{-2}$  Earth masses acquires a tenuous atmosphere of gas from the disk. Fragments are captured by the atmosphere even if they do not collide directly with the embryo, implying that the collisional cross section of the embryo is enhanced. This effect advances the growth of Mars-mass or larger embryos (Inaba & Ikoma 2003). Embryos with the atmospheres accrete fragments prior to their drift inward and can acquire more than 10 Earth masses starting from 10km-sized planetesimals (Inaba et al. 2003). However, erosive collisions and initial planetesimal sizes strongly affect final embryo masses (Kobayashi et al. 2010).

This paper investigates the embryo growth taking into account erosive collisions and embryo's atmosphere. Although growing embryos may fall into a central star due to the type I migration (e.g., Tanaka et al. 2002), we neglect the migration here. We perform both analytical studies and statistic simulations, which extend those of Kobayashi et al. (2010) by including atmospheric enhancement of embryo growth. The goal is to find out what determines embryo growth and whether an embryo can reach the critical core mass. We introduce the theoretical model in Section 2 and derive final embryo masses taking into account atmosphere in Section 3. In Section 4, we check solutions for final masses against the statistical simulations. Sections 5 and 6 contain a discussion and a summary of our findings.

## 2. THEORETICAL MODEL

### 2.1. Disk Model

We introduce a power-law disk model for the initial surface mass density of solids  $\Sigma_{s,0}$  and gas  $\Sigma_{g,0}$  such that

$$\Sigma_{s,0} = f_{\text{ice}} \Sigma_1 \left( \frac{a}{1 \text{ AU}} \right)^{-q} \text{ g cm}^{-2}, \quad (1)$$

$$\Sigma_{g,0} = f_{\text{gas}} \Sigma_1 \left( \frac{a}{1 \text{ AU}} \right)^{-q} \text{ g cm}^{-2}, \quad (2)$$

where  $a$  is a distance from a central star,  $\Sigma_1$  is the reference surface density at 1 AU, and  $q$  is the power-law index of the radial distribution. The gas-dust ratio  $f_{\text{gas}} = 240$  (Hayashi 1981). The factor  $f_{\text{ice}}$  that represents the increase of solid density by ice condensation beyond the snow line  $a_{\text{ice}}$  is given by  $f_{\text{ice}} = 1$  ( $a < a_{\text{ice}}$ ) and 4.2 ( $a \geq a_{\text{ice}}$ ). In the MMSN model,  $\Sigma_1 = 7.1 \text{ g cm}^{-2}$  and  $q = 3/2$ . If the disk is optically thin,

$$a_{\text{ice}} = 2.7 \left( \frac{L_*}{L_\odot} \right)^{1/2} \text{ AU}, \quad (3)$$

where  $L_*$  and  $L_\odot$  are the luminosities of the central star and the sun, respectively. In reality, disks may be optically thick even after planetesimal formation. However, we assume Equation (3) for simplicity.

### 2.2. Fragmentation Outcome Model

Kobayashi & Tanaka (2010) showed erosive collisions to dominate the collision cascade. We should take into account such collisions properly. We assume that fragmentation outcomes are scaled by the impact energy and hence the total ejecta mass  $m_e$  produced by a single collision between  $m_1$  and  $m_2$  is given by a function of the dimensionless impact energy  $\phi = m_1 m_2 v^2 / 2(m_1 + m_2)^2 Q_D^*$ , where  $v$  is the collisional velocity between  $m_1$  and  $m_2$  and  $Q_D^*$  is the specific energy needed for  $m_e = (m_1 + m_2)/2$ . Following Kobayashi & Tanaka (2010) and Kobayashi et al. (2010), we model

$$\frac{m_e}{m_1 + m_2} = \frac{\phi}{1 + \phi}. \quad (4)$$

Inaba et al. (2003) derived  $m_e$  from the fragment model developed by Wetherill & Stewart

(1993) with a value of  $Q_D^*$  found by Benz & Asphaug (1999) for ice. Fig. 1 shows their model and Equation (4). As discussed in Kobayashi & Tanaka (2010), most of the laboratory experiments and the hydrodynamic numerical simulations of collisional disruption showed  $m_e$  not to have a discontinuity at  $\phi = 1$  (Housen et al. 1991; Takagi et al. 1984; Benz & Asphaug 1999). Therefore, Equation (4) includes erosive collisions ( $\phi < 1$ ) more accurately.

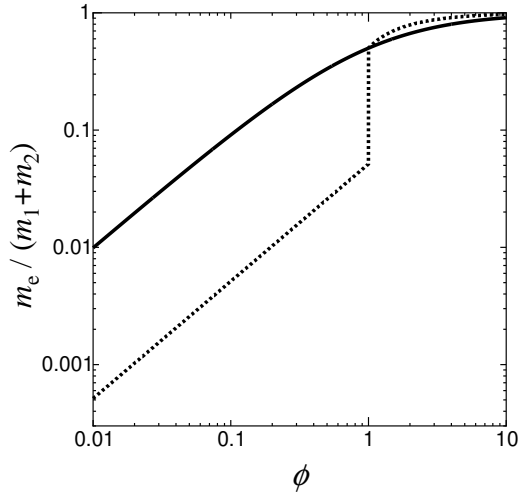


Fig. 1.— The total ejecta mass  $m_e$  produced by a single collision with  $m_1$  and  $m_2$ , as a function of the dimensionless energy  $\phi = m_1 m_2 v^2 / 2(m_1 + m_2)^2 Q_D^*$ . The solid line indicates Equation (4). For reference, the dotted lines are shown for the fragment model of Inaba et al. (2003) with  $m_1 = 10^3 m_2 = 4.2 \times 10^{20}$  g.

The critical energy  $Q_D^*$  is given by

$$Q_D^* = Q_{0s} \left( \frac{r}{1 \text{ cm}} \right)^{\beta_s} + Q_{0g} \rho_p \left( \frac{r}{1 \text{ cm}} \right)^{\beta_g} + C_{gg} \frac{2Gm}{r}, \quad (5)$$

where  $r$  and  $m$  are the radius and mass of a body,  $\rho_p$  is its density, and  $G$  is the gravitational constant. The first term on the right-hand side of Equation (5) is dominant for  $r \lesssim 10^4$ – $10^5$  cm, the second term describes  $Q_D^*$  of  $r \lesssim 10^7$  cm, and the third term controls  $Q_D^*$  for the larger bodies. Benz & Asphaug (1999) performed the hydrodynamical simulations of collisional dispersion for  $r = 1$ – $10^7$  cm and provided the values of  $Q_{0s}$ ,  $\beta_s$ ,  $Q_{0g}$ , and  $\beta_g$ . For  $r \gtrsim 10^7$  cm,  $Q_D^*$  is purely

determined by the gravitational binding energy, being independent of material properties. The collisional simulation for gravitational aggregates yields  $C_{gg} \sim 10$  (Stewart & Leinhardt 2009).

### 2.3. Enhancement Radius by Atmosphere

Once a planetary embryo has grown larger than the Moon, it acquires an atmosphere. It helps the accretion of planetesimals or fragments onto an embryo; small bodies are captured by the atmosphere of the embryo.

Inaba & Ikoma (2003) provided an analytical model for a density profile of the atmosphere. We consider the atmosphere at a distance  $R_e$  from an embryo center. We assume that  $R_e$  is much smaller than that at the outer boundary of the atmosphere and that its temperature is much higher than that at the boundary. The atmospheric density  $\rho_a$  is then proportional to  $R_e^{-3}$  (Mizuno 1980; Stevenson 1982). Applying the temperature  $T_{\text{neb}}$ , pressure  $P_{\text{neb}}$ , and density  $\rho_{\text{neb}}$  of the nebula in the disk midplane as those at the outer boundary of atmosphere, the density profile of the atmosphere around an embryo with mass  $M$  is given by

$$\frac{\rho_a(R_e)}{\rho_{\text{neb}}} = \frac{16\pi\sigma_{\text{SB}}GM T_{\text{neb}}^4}{3\kappa L_e P_{\text{neb}}} \left( \frac{GM\rho_{\text{neb}}}{4P_{\text{neb}}R_e} \right)^3, \quad (6)$$

where  $\kappa$  is the opacity of the atmosphere and  $\sigma_{\text{SB}}$  is the Stephan-Boltzmann constant. The planetary luminosity  $L_e$  mainly comes from the accretion of bodies. We approximate

$$L_e = \frac{GM}{R} \frac{dM}{dt}, \quad (7)$$

where  $R$  is the embryo radius. To validate the assumption of  $\rho_a \propto R_e^{-3}$ , we will apply the complete model by Inaba & Ikoma (2003) to our statistic simulation and compare our analytical solutions with the statistical simulations in Section 4.

When a body passes by a planetary embryo with an atmosphere, the embryo can accrete the body without direct collision due to the atmosphere. The relative velocity between the body and the embryo at infinity is determined by the eccentricity  $e$  of the small body; it is given by  $ev_k$  with the Keplerian velocity  $v_k = \sqrt{GM_*/a}$  and  $M_*$  being the mass of a central star. The relative velocity is typically smaller than the surface

escape velocity of the embryo during the embryo growth. If the orbital energy of a body is sufficiently reduced by the atmospheric gas drag, the body is captured by the embryo. The maximum radius  $r$  of bodies captured at distance  $R_e$  is given by (Inaba & Ikoma 2003)

$$r = \frac{9ah_M}{6 + \tilde{e}^2} \frac{\rho_a(R_e)}{\rho_p}, \quad (8)$$

where  $h_M = (M/3M_*)^{1/3}$  is the reduced Hill radius of the embryo and  $\tilde{e} = e/h_M$ . Equation (8) is derived under the two-body approximation. Tanigawa & Ohtsuki (2010) confirmed that Equation (8) is valid in the case where the three-body effects are included.

Equation (8) means that  $R_e$  is the effective collisional radius of an embryo for bodies with radius  $r$ . The enhanced radius of the embryo with atmosphere is thus derived from Eqs. (6)–(8) as

$$\frac{R_e}{R} = \frac{FM^{8/9}}{m^{1/9}\dot{M}^{1/3}}, \quad (9)$$

where

$$F = \left[ \frac{\pi^2 a \sigma_{\text{SB}} T_{\text{neb}}^4 \rho_{\text{neb}}^4 G^3}{(\tilde{e}^2 + 6)(3M_*)^{1/3} \kappa P_{\text{neb}}^4} \right]^{1/3}. \quad (10)$$

The enhancement factor  $R_e/R$  given by Equation (9) is shown in Fig. 2, where the power-law density profile given by Equation (6) is compared with a more realistic profile given by Inaba & Ikoma (2003). As we discuss later, planetary embryos mainly grow through collisions with planetesimals of the initial size or with fragments of radius  $r \sim 10$  m. The enhancement factor calculated with Equation (9) reproduces well the more realistic one for km-sized or larger planetesimals, but Equation (9) significantly overestimates  $R_e/R$  for fragments. However, since the accretion rate due to collision with such fragments has a weak dependence on the enhancement factor ( $\propto (R_e/R)^{1/2}$ ; see Equation (30)), this discrepancy produces insignificant errors.

### 3. FINAL EMBRYO MASS

#### 3.1. Isolation Mass

Planetary embryos can grow until they have accreted all planetesimals within their feeding

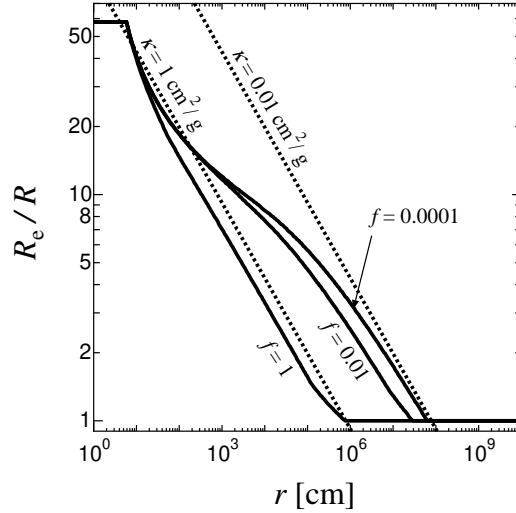


Fig. 2.— The ratio of the enhanced radius of planetary embryo to its physical radius with  $M = M_\oplus$ ,  $\rho_p = 1 \text{ g cm}^{-3}$ , and  $\dot{M} = 1 \times 10^{-6} M_\oplus/\text{yr}$  for  $\tilde{e} = 4$  in the MMSN disk around the star with mass  $M_\odot$ . The ratios are calculated by the formulae of Inaba & Ikoma (2003) for the opacity obtained from Equation (39) with the grain depletion factor  $f = 10^{-4}$ –1 (solid lines) and by Equation (9) for the constant opacity  $\kappa = 0.01 \text{ cm}^2 \text{ g}^{-1}$  and  $1 \text{ cm}^2 \text{ g}^{-1}$  (dotted lines).

zones. The width of a feeding zone is given by the orbital separation of neighboring embryos,  $\tilde{b}(2M/3M_*)^{1/3}a$ , where  $\tilde{b} \simeq 10$  is the separation measured in their mutual Hill radii (Kokubo & Ida 2000, 2002). The maximum mass or “isolation mass” is  $M_{\text{iso}} = 2\pi a^2 (2M_{\text{iso}}/3M_*)^{1/3} \tilde{b} \Sigma_{s,0}$ . It can be expressed as

$$M_{\text{iso}} = 2.8 \left( \frac{\tilde{b}}{10} \right)^{3/2} \left( \frac{\Sigma_{s,0}}{2.7 \text{ g cm}^{-2}} \right)^{3/2} \times \left( \frac{a}{5 \text{ AU}} \right)^3 \left( \frac{M_*}{M_\odot} \right)^{-1/2} M_\oplus, \quad (11)$$

where  $M_\oplus$  is the Earth mass and  $M_\odot$  is the solar mass. The planetary embryo mass approaches the isolation mass if fragmentation is ignored (Kokubo & Ida 2000, 2002). However, if fragmentation is included, the embryo mass can reach only about Mars mass for a MMSN disk (Kobayashi et al. 2010).

### 3.2. Planetesimal Accretion

As shown by Kobayashi et al. (2010), a planetary embryo accretes planetesimals with masses comparable to original ones or fragments resulting from collisional grinding of planetesimals. In the former case, a final embryo mass is determined by the equilibrium between the accretion of planetesimals and their removal due to collisional grinding. In the latter case, an embryo can grow until fragments are depleted by the gas drag. Following Kobayashi et al. (2010), we want here to derive final masses determined by the accretion of planetesimals in the case with atmospheric enhancement, while we treat the fragment accretion in Section 3.3.

At the oligarchic stage, embryos mainly grow through collisions with planetesimals that dominate the surface density. The growth rate of an embryo with mass  $M$  is given by

$$\frac{dM}{dt} = C_{\text{acc}} \Sigma_s a^2 h_M^2 \langle P_{\text{col}} \rangle \Omega_k, \quad (12)$$

where  $\Omega_k$  is the Keplerian frequency and  $C_{\text{acc}}$  is the correction factor on the order of unity. The dimensionless collision rate  $\langle P_{\text{col}} \rangle$  is formulated as a function of the eccentricities  $e$  and inclinations  $i$  of bodies accreted onto the embryo. We assume  $e = 2i$  in this analysis.

Embryos have a constant ratio of their separations to their Hill radii (Kokubo & Ida 1998). When the ratio decreases as embryos grow, relatively smaller embryos are culled and thereby remaining embryos keep the ratio constant. Supposing the cull occurs instantaneously, the growth rate of embryos due to the cull is estimated to be a half of that from planetesimals. Therefore, we set  $C_{\text{acc}} = 1.5$  (e.g., Chambers 2006; Kobayashi et al. 2010).

For kilometer-sized or larger planetesimals, their eccentricities  $e$  are controlled by the embryo stirring and gas drag. The stirring rate is written as  $de^2/dt = n_M a^2 h_M^4 \langle P_{\text{VS}} \rangle \Omega_k$ , where  $n_M$  is the surface number density of embryos and the dimensionless stirring rate  $\langle P_{\text{VS}} \rangle$  is given by  $\langle P_{\text{VS}} \rangle = C_{\text{VS}} h_M^2 \ln(\Lambda^2 + 1)/e^2$  with  $C_{\text{VS}} = 40$  and  $\Lambda = 5\tilde{e}^3/96$  for  $e \gg h_M$  (Ohtsuki et al. 2002). Although  $\ln(\Lambda^2 + 1)$  in  $\langle P_{\text{VS}} \rangle$  is weakly dependent on  $e$ , we adopt, in this analysis,  $\ln(\Lambda^2 + 1) \simeq 8$ , with which value we can reproduce the formula of Ohtsuki et al. (2002) for  $\tilde{e} = 3$ –10. The gas-drag

time  $\tau$  is characterized as (Adachi et al. 1976)

$$\tau = \frac{2m}{\pi r^2 C_D \rho_{\text{neb}} v_k}, \quad (13)$$

where the dimensionless gas drag coefficient  $C_D = 0.5$  for km-sized or larger planetesimals. It should be noted that  $\tau$  is the stopping time due to gas drag only when the relative velocity  $u$  between gas and a body is equal to the Keplerian velocity; hence  $\tau$  is almost always much shorter than the stopping time for realistic relative velocities. The  $e$ -damping rate due to gas drag is given by  $de^2/dt = -C'_{\text{gas}} e^3/\tau$  with  $C'_{\text{gas}} = 2.1$  (Inaba et al. 2001). Using  $n_M = (2\pi a \delta a)^{-1}$  with the orbital separation of neighboring embryos of  $\delta a = 2^{1/3} h_M a \tilde{b}$  (Kokubo & Ida 2000) and equating the stirring and damping rates result in the equilibrium eccentricity:<sup>1</sup>

$$\tilde{e} = \left[ \frac{C_{\text{VS}} \ln(\Lambda^2 + 1) \Omega_k \tau}{2^{4/3} \pi \tilde{b} C_{\text{gas}}} \right]^{1/5}. \quad (14)$$

Since we roughly estimate  $\tilde{e} \sim (\tau \Omega_k)^{1/5}$  from Equation (14), the eccentricities of the kilometer-sized and larger bodies are larger than  $h_M$ , according to the assumption  $e \gg h_M$ .

Taking into account the enhancement due to the atmosphere, the dimensionless collisional probability for  $e \gg h_M$  is given by (Greenzweig & Lissauer 1992; Inaba et al. 2001; Inaba & Ikoma 2003)

$$\langle P_{\text{col}} \rangle = \frac{C_{\text{col}} \tilde{R}}{\tilde{e}^2} \frac{R_e}{R}, \quad (15)$$

where  $C_{\text{col}} = 36$  and  $\tilde{R} = R/ah_M = (9M_*/4\pi\rho_p)^{1/3}/a$ . Inserting Eqs. (9) and (15) to Equation (12), we obtain  $\dot{M}$  as

$$\frac{dM}{dt} = A_{\text{ca}} M^{7/6} \Sigma_s^{3/4}, \quad (16)$$

where

$$A_{\text{ca}} = \left[ \frac{C_{\text{acc}} a^2 C_{\text{col}} \tilde{R} F \Omega_k}{(3M_*)^{2/3} \tilde{e}^2 m^{1/9}} \right]^{3/4}. \quad (17)$$

<sup>1</sup>Ida & Makino (1993) and Thommes et al. (2003) presented a similar equation from the stirring timescale derived by Ida & Makino (1993). We apply the formula of Ohtsuki et al. (2002), which weakly depends on  $e$  through  $\ln(\Lambda^2 + 1)$ . However, since we adopt a constant value for  $\ln(\Lambda^2 + 1)$  in this analysis, there is no substantial difference between their and our treatment, except for the definition of the coefficient for the viscous stirring.

As embryos grow, destructive collisions between planetesimals are induced by the stirring of embryos and generate a lot of small fragments, which produce further small bodies through mutual collisions. Since very small bodies resulting from successive collisions are rapidly removed by the gas drag, the collision cascade reduces the surface density of solids. In the collision cascade, collisional fragmentation dominates the mass flux along the mass coordinate. Since the mass flux is independent of mass in a steady state, the mass distribution of fragments follows a power law and the power-law exponent  $\alpha$  is given by  $\alpha = (11 + 3p)/(6 + 3p)$  for  $e^2/Q_D^* \propto m^{-p}$  (Kobayashi & Tanaka 2010). The steady-state mass flux determines the surface density reduction as (Kobayashi & Tanaka 2010; Kobayashi et al. 2010)

$$\frac{d\Sigma_s}{dt} = -B_{ca}\Sigma_s^2 M^{2(\alpha-1)/3}. \quad (18)$$

$$B_{ca} = \frac{(2-\alpha)^2 \Omega_k s_{123}(\alpha)}{m^{1/3}} \times \left( \frac{\tilde{e}^2 v_k^2}{2(3M_*)^{2/3} Q_D^*} \right)^{\alpha-1}, \quad (19)$$

where

$$s_{123}(\alpha) = \int_0^\infty \left[ \frac{\phi}{2-b} - \phi \ln \frac{\epsilon\phi}{(1+\phi)^2} + \ln(1+\phi) \right] \times \frac{\phi^{-\alpha}}{1+\phi} d\phi, \quad (20)$$

and  $h_0 = 1.1\rho_p^{-2/3}$ . For the derivation of Equation (18), we apply the fragmentation outcome model of Kobayashi & Tanaka (2010); ejecta yielded by a single collision between  $m_1$  and  $m_2$  are characterised by their total mass  $m_e$  and their power-law mass spectrum with an exponent  $b$  below the mass  $m_L = \epsilon(m_1 + m_2)\phi/(1+\phi)^2$ , where  $\epsilon < 1$  is a constant. The  $\Sigma_s$  reduction rate is insensitive to  $\epsilon$  and  $b$  (Kobayashi & Tanaka 2010). We set  $b = 5/3$  and  $\epsilon = 0.2$  in this paper.

Dividing Equation (16) by Equation (18) and integrating, we obtain the relation between the embryo mass  $M$  and the surface density  $\Sigma_s$ :

$$\begin{aligned} \frac{6}{4\alpha-5} \left[ M^{(4\alpha-5)/6} - M_0^{(4\alpha-5)/6} \right] \\ = 4(\Sigma_s^{-1/4} - \Sigma_{s,0}^{-1/4}) \frac{A_{ca}}{B_{ca}}, \end{aligned} \quad (21)$$

where  $M_0$  is the initial embryo mass. Note that the derivation of Equation (21) assumed that the planetesimal density reduction is caused by collisional grinding, but the planetesimal accretion onto embryos significantly contributes to the  $\Sigma_s$ -reduction when the surface density of planetesimals,  $\Sigma_s$ , is much smaller than that of embryos,  $Mn_M$ . When an embryo reaches a final mass  $M_{ca}$ ,  $\Sigma_s$  may be described as  $C_{\Sigma_s} M_{ca} n_M$  with a constant  $C_{\Sigma_s} \ll 1$ ; hence

$$\frac{\Sigma_s}{\Sigma_{s,0}} = C_{\Sigma_s} \left( \frac{M_{ca}}{M_{iso}} \right)^{2/3}. \quad (22)$$

For  $C_{\Sigma_s} \sim 0.1$ , a final mass is consistent with simulations (Kobayashi et al. 2010). We thus set  $C_{\Sigma_s} = 0.1$  to derive a final mass. From Eqs. (21) and (22), we obtain a final embryo mass

$$M_{ca} = \left[ \frac{2(4\alpha-5)A_{ca}C_{\Sigma_s}^{-1/4}\Sigma_{s,0}^{-1/4}M_{iso}^{1/6}}{3B_{ca}} \right]^{3/2(\alpha-1)}. \quad (23)$$

Here, we assume  $M_{ca} \gg M_0$ .

For kilometer-sized or larger planetesimals,  $Q_D^* = Q_{0g}\rho_p r^{\beta_g}$  with constants  $Q_{0g}$  and  $\beta_g$ . We apply  $Q_{0g} = 2.1 \text{ erg cm}^3 \text{ g}^{-2}$  and  $\beta_g = 1.19$  for ice (Benz & Asphaug 1999) and  $\tilde{e}^2 \gg 6$ , and Equation (23) can then be re-written as

$$\begin{aligned} M_{ca} = & 1.8 \times 10^{-2} \left( \frac{a}{5 \text{ AU}} \right)^{2.8} \left( \frac{m}{4 \times 10^{20} \text{ g}} \right)^{0.63} \\ & \times \left( \frac{Q_{0g}}{2.1 \text{ erg cm}^3 \text{ g}^{-2}} \right)^{1.5} \left( \frac{\kappa}{0.01 \text{ g cm}^{-2}} \right)^{-0.51} \\ & \times \left( \frac{f_{\text{gas}}\Sigma_1}{1.7 \times 10^3 \text{ g cm}^{-2}} \right)^{1.41} M_\oplus. \end{aligned} \quad (24)$$

Since planetesimals grow before planetesimals' fragmentation starts, planetesimal mass  $m$  is slightly larger than initial planetesimal mass  $m_0$ . Kobayashi et al. (2010) showed that planetesimals mainly accreting onto embryos have  $m = 100m_0$ . For  $m_0 \gtrsim 10^{23} \text{ g}$  ( $r_0 \gtrsim 3 \times 10^3 \text{ km}$ ), final embryo masses exceed  $10 M_\oplus$  at 5 AU in a MMSN disk, but embryos cannot reach it within a disk lifetime due to their slow growth. The final mass  $M_{ca}$  is independent of  $\Sigma_{s,0}$ , while high  $\Sigma_{g,0}$  increases  $M_{ca}$  because gas drag highly damps  $\tilde{e}$ . For  $\Sigma_1 = 71 \text{ g cm}^{-2}$  ( $10\times\text{MMSN}$ ), initial planetesimals with  $r_0 \gtrsim 50 \text{ km}$  can produce an embryo with  $10 M_\oplus$  at 5 AU.

For comparison, we also show the final mass  $M_c$  in the same situation but neglecting the atmosphere (Kobayashi et al. 2010):

$$M_c = 0.10 \left( \frac{a}{5 \text{ AU}} \right)^{0.63} \left( \frac{m}{4 \times 10^{20} \text{ g}} \right)^{0.48} \times \left( \frac{\ln(\Sigma_{s,0}/\Sigma_s)}{4.5} \right)^{1.21} \left( \frac{Q_{0g}}{2.1 \text{ erg cm}^3 \text{ g}^{-2}} \right)^{0.89} \times \left( \frac{f_{\text{gas}} \Sigma_1}{1.7 \times 10^3 \text{ g cm}^{-2}} \right)^{1.21} M_\oplus, \quad (25)$$

where  $\ln(\Sigma_{s,0}/\Sigma_s) \simeq 4.5$  is estimated from Equation(22) with  $C_{\Sigma_s} = 0.1$  for  $M = 0.1 M_\oplus$  in the MMSN model. The collisional enhancement due to the atmosphere is inefficient for  $m = 4 \times 10^{20} \text{ g}$ ;  $M_{\text{ca}} < M_a$ . If  $m \gtrsim 4 \times 10^{22} \text{ g}$ , the atmosphere contributes to embryo growth.

### 3.3. Fragment Accretion

As described above, planetesimals are ground down by collision cascade and resulting small fragments spiral into the central star by gas drag. In the steady state of collision cascade, the surface density of planetesimals is much larger than that of fragments. However, when the grinding of planetesimals is much quicker than the removal of small fragments by gas drag, fragments accumulate at the low-mass end of collision cascade and determine the total mass of bodies. Embryos then grow through the accretion of such fragments.

The specific impact energy between equal-sized bodies,  $e^2 v_k^2/8$ , should be much smaller than  $Q_D^*$  at the low-mass end; thus the typical fragments at the low-mass end have

$$e^2 v_k^2 = C_L Q_D^*, \quad (26)$$

where  $C_L \sim 1$  is a constant. Although Kobayashi et al. (2010) used  $C_L = 1$  to determine the typical fragment mass, we apply  $C_L = 0.5$  to correct a mistake of factor 2 in their  $e^2$ . Such small fragments feel strong gas drag in Stokes regime;  $C_D = 5.5 c l_g / u r$ , where  $c$  is the sound velocity and  $l_g = l_{g,0} / \rho_g$  is the mean free path of gas molecules with  $l_{g,0} = 1.7 \times 10^{-9} \text{ g cm}^{-2}$  (Adachi et al. 1976). The eccentricities of fragments at the low-mass end are much smaller than  $h_M$  and  $\eta$ , where  $\eta = (v_k - v_{\text{gas}})/v_k$  is the deviation of the gas rotation velocity  $v_{\text{gas}}$  from the

Keplerian velocity. The dimensionless viscous stirring rate is given by  $\langle P_{\text{VS}} \rangle = \langle P_{\text{VS,low}} \rangle = 73$  for  $e \ll h_M$  (Ohtsuki et al. 2002) and the damping rate is expressed as  $de^2/dt = -2\eta e^2/\tau$  for  $e \ll \eta$  (Adachi et al. 1976). The equilibrium eccentricity between stirring by embryos and damping by gas drag is obtained as (Kobayashi et al. 2010)

$$e^2 = \frac{h_M^3 \langle P_{\text{VS,low}} \rangle \tau \Omega_K}{27^{1/3} \pi \tilde{b} \eta}, \quad (27)$$

Using Eqs. (13), (26), and (27) under the Stokes regime, we have the fragment mass  $m_f$  at the low-mass end of collision cascade:

$$m_f = m_{f0} M^{-3/2}, \quad (28)$$

where

$$m_{f0} = \left[ \frac{221 M_* \tilde{b} C_L Q_D^*}{\langle P_{\text{VS,low}} \rangle a^2 \Omega_K^3} \frac{c}{l_{g,0}} \left( \frac{3}{4\pi \rho_p} \right)^{1/3} \right]^{3/2}. \quad (29)$$

For  $e \ll h_M$ , Ida & Nakazawa (1989) found that the dimensionless collision rate for  $e \ll h_M$  is given by  $\langle P_{\text{col,low}} \rangle = 11.3 \sqrt{\tilde{R}}$ , where the coefficient is determined by Inaba et al. (2001). Since the atmosphere effectively enhances an embryo radius for the accretion of bodies, the collision rate is modified to be (Inaba & Ikoma 2003)

$$\langle P_{\text{col}} \rangle = \langle P_{\text{col,low}} \rangle \sqrt{\frac{R_e}{R}}. \quad (30)$$

We obtain the accretion rate of fragments by an embryo,  $\dot{M}$ , from Eqs. (12) and (30) as

$$\frac{dM}{dt} = A_{\text{fa}} M^{43/42} \Sigma_s^{6/7}, \quad (31)$$

$$A_{\text{fa}} = \left[ \frac{F^{1/2} \langle P_{\text{col,low}} \rangle C_{\text{acc}} a^2 \Omega_K}{m_{f0}^{1/18} (3M_*)^{2/3}} \right]^{6/7}. \quad (32)$$

Fragments with  $m_f$  at the low-mass end of collision cascade that dominate the surface density of solids  $\Sigma_s$  are no longer disrupted by collisions and drift inward by gas drag. The drift velocity is given by  $2\eta^2 a/\tau$  and then the  $\Sigma_s$ -reduction rate due to the radial drift is expressed as  $d\Sigma_s/dt = -2(9/4 - q)\eta^2 \Sigma_s/\tau$  with the assumption of  $\Sigma_s \propto a^{-q}$ . Since  $\tau$  of fragments with  $m_f$  is determined by Equations (26) and (27), we have



(Kobayashi et al. 2010)

$$\frac{d\Sigma_s}{dt} = -B_{fa}\Sigma_s M, \quad (33)$$

$$B_{fa} = \left(\frac{9}{4} - q\right) \frac{\langle P_{vs,low} \rangle \Omega_k \eta v_k^2}{2^{4/3} 3\pi M_* C_L \tilde{b} Q_D^*}. \quad (34)$$

Since fragments are later produced by embryo growth in an outer disk, the radial distribution depends on time in contrast to the assumption of  $\Sigma_s \propto a^{-q}$ . Nevertheless, the effect is negligible for embryo growth unless the atmosphere is considered (Kobayashi et al. 2010). We discuss this effect with the atmospheric enhancement in §4 and §5.

We can now obtain the final embryo mass  $M_{fa}$  from  $\dot{M}$  and  $\dot{\Sigma}_s$  for fragment accretion, similar to the case of planetesimal accretion. Integration of Equation (31) divided by Equation (18) results in

$$M_{fa} = \left(\frac{41A_{fa}}{36B_{fa}}\right)^{42/41} \Sigma_{s,0}^{36/41}, \quad (35)$$

where we assume  $M_{fa} \gg M_0$  and  $\Sigma_{s,0} \gg \Sigma_s$ . For  $q = 3/2$ , we have

$$\begin{aligned} M_{fa} &= 0.20 \left(\frac{a}{5 \text{ AU}}\right)^{117/164} \left(\frac{\kappa}{0.01 \text{ g cm}^{-3}}\right)^{1/7} \\ &\times \left(\frac{f_{ice}\Sigma_1}{30 \text{ g cm}^{-2}}\right)^{36/41} \\ &\times \left(\frac{Q_D^*}{3.1 \times 10^6 \text{ erg g}^{-1}}\right)^{42/41} M_{\oplus}. \end{aligned} \quad (36)$$

Here, we adopted  $f_{ice}$  and  $\Sigma_1$  for the minimum mass solar nebula model. The weak dependence of  $M_{fa}$  on  $\kappa$  implies that the overestimate of  $R_e/R$  due to the power-law radial profile is insignificant, as discussed in Section 2.3.

For the case without an atmosphere, Kobayashi et al. (2010) derived a final mass for the fragment accretion,

$$\begin{aligned} M_f &= 0.14 \left(\frac{a}{5 \text{ AU}}\right)^{3/8} \left(\frac{f_{ice}\Sigma_1}{30 \text{ g cm}^{-2}}\right)^{3/4} \\ &\times \left(\frac{Q_D^*}{3.1 \times 10^6 \text{ erg g}^{-1}}\right)^{3/4} M_{\oplus}. \end{aligned} \quad (37)$$

Eqs. (36) and (37) imply that the final masses increase due to the atmosphere, but the enhancement is insignificant;  $M_{fa}/M_f \simeq 1.4\text{--}2$  for  $1\text{--}10 \times \text{MMSN}$ .

If we neglect the collisional enhancement due to atmosphere, the final mass  $M_{na}$  is determined by the larger of  $M_c$  and  $M_f$  (Kobayashi et al. 2010). In the case with atmosphere, a final mass  $M_a$  is also given by the larger of  $M_{ca}$  and  $M_{fa}$ . The final mass  $M_a$  is shown in Figs. 3–5. For the initial planetesimal radius  $r_0 = 10 \text{ km}$ ,  $M_a$  is dominated by  $M_{fa}$  inside the point where the line of  $M_a$  bends in Fig. 3 and by  $M_{ca}$  outside. The final mass  $M_a$  is determined only by  $M_{fa}$  for  $r_0 = 1 \text{ km}$  (Fig. 4) and by  $M_{ca}$  for  $r_0 = 100 \text{ km}$  (Fig. 5) in the range of interest.

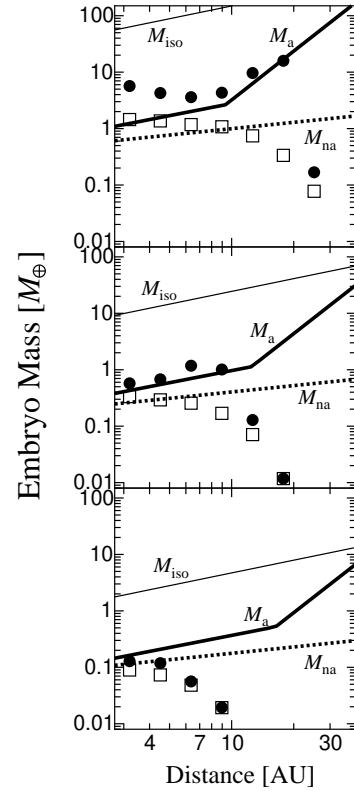


Fig. 3.— Embryo masses with (circles) and without (squares) atmosphere after  $10^7$  years for  $m_0 = 4.2 \times 10^{18} \text{ g}$  ( $r_0 = 10 \text{ km}$ ), as a function of distance from the central star. We set  $\Sigma_1 = 71 \text{ g cm}^{-2}$  (top),  $\Sigma_1 = 21 \text{ g cm}^{-2}$  (middle), and  $\Sigma_1 = 7.1 \text{ g cm}^{-2}$  (bottom). Solid lines indicate  $M_a$  which is the larger of  $M_{ca}$  and  $M_{fa}$  for  $\kappa = 0.01 \text{ cm}^2 \text{ g}^{-1}$ . Dotted lines represent  $M_{na}$  which is the larger of  $M_c$  and  $M_f$ . Thin lines show  $M_{iso}$ .

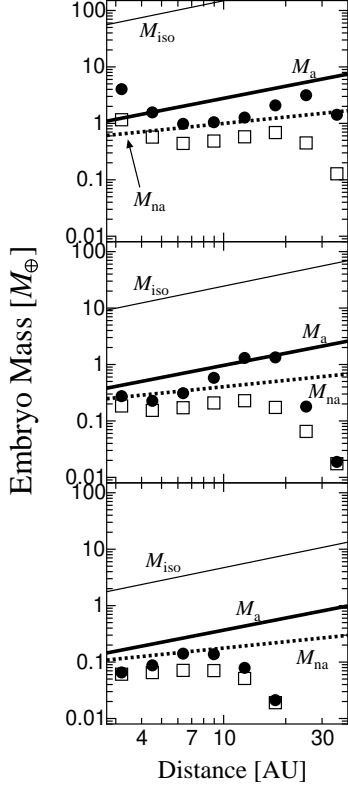


Fig. 4.— Same as Fig. 3, but for  $m_0 = 4.2 \times 10^{15}$  g (radii of 1 km).

#### 4. NUMERICAL SIMULATION

Regarding the method of numerical simulation, we basically follow Kobayashi et al. (2010). The method of Kobayashi et al. (2010) is briefly explained here. In the calculation, a disk is divided into concentric annuli and each annulus contains a set of mass batches. We set the mass ratio between the adjacent batches to 1.2, which can reproduce the collisional growth of bodies resulting from  $N$ -body simulation without fragmentation (Kobayashi et al. 2010) and the analytical solution of mass depletion due to collisional grinding (Kobayashi & Tanaka 2010). The mass and velocity evolution of bodies and their radial transport are calculated as follows.

- The mass distribution of bodies evolves through their mutual collisions that produce mergers and fragments. The total mass of fragments ejected by a single collision is

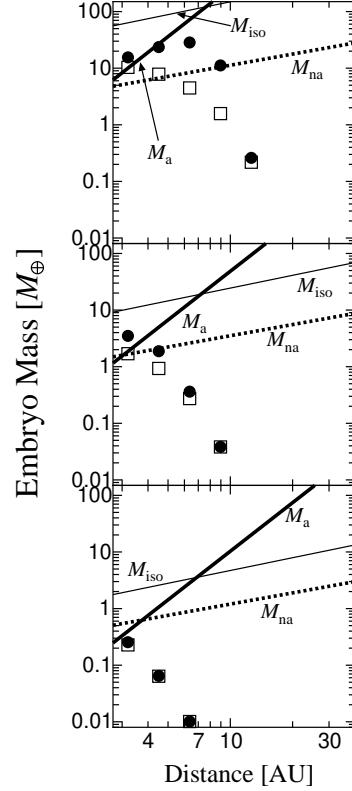


Fig. 5.— Same as Fig. 3, but for  $m_0 = 4.2 \times 10^{21}$  g (radii of 100 km).

given by Equation (4) and the remnant becomes a merger. The collision rates between the bodies are calculated from the formulae of Inaba et al. (2001).

- The random velocities given by  $e$  and  $i$  of the bodies simultaneously evolve through their mutual gravitational interactions, gas drag, and collisional damping. The formulae of Ohtsuki et al. (2002) are applied to describe the changing rates of  $e$  and  $i$ . The gas-drag damping rates of  $e$  and  $i$  are described as functions of  $e$ ,  $i$ ,  $\eta$ , and  $\tau$  according to Inaba et al. (2001). To determine  $\tau$ , we take into account Stokes and Epstein drag as well as a drag law with a quadratic dependence on velocity. For the collisional damping, both fragments and a merger resulting from a single collision have the velocity dispersion at the gravity center of colliding bodies.

- In each annulus there is a loss and gain of bodies due to their inward drift. The number loss rate from an annulus is given by  $\int (N(m)v_{\text{drift}}/\Delta a)dm$ , where  $v_{\text{drift}}$  is the drift velocity of bodies,  $N(m)dm$  is the number of bodies with mass ranging from  $m$  to  $m + dm$  in the annulus, and  $\Delta a$  is the width of the annulus. The bodies lost from each annulus are added to the next inner annulus. The drift velocity is given by (Kobayashi et al. 2010)

$$v_{\text{drift}} = \frac{2a\eta}{\tau} \frac{\tilde{\tau}_{\text{stop}}^2}{1 + \tilde{\tau}_{\text{stop}}^2} \left[ \frac{(2E + K)^2}{9\pi^2} e^2 + \frac{4}{\pi^2} i^2 + \eta^2 \right]^{1/2} \quad (38)$$

where  $E = 2.157$ ,  $K = 1.211$  and the dimensionless stopping time  $\tilde{\tau}_{\text{stop}} = \Omega_k \tau / (e + i + \eta)$  is adopted.

In this paper, we add a collisional enhancement due to the atmosphere. Although the simple power-law radial density profile of the atmosphere (Equation (6)) is used for the derivation of final masses ( $M_{\text{ca}}$ ,  $M_{\text{fa}}$ ), the simulation incorporates a more realistic profile provided by the formulae of Inaba & Ikoma (2003). The opacity of the embryo's atmosphere in their model is given by  $\kappa = \kappa_{\text{gas}} + f\kappa_{\text{gr}}$ , where  $\kappa_{\text{gas}}$  is the gas opacity,  $\kappa_{\text{gr}}$  is the opacity of grains having an interstellar size distribution, and  $f$  is the grain depletion factor. Following Inaba & Ikoma, we adopt

$$\kappa = \begin{cases} 0.01 + 4f \text{ cm}^2 \text{ g}^{-1} & \text{for } T \leq 170 \text{ K}, \\ 0.01 + 2f \text{ cm}^2 \text{ g}^{-1} & \text{for } 170 \text{ K} < T \leq 1700 \text{ K}, \\ 0.01 \text{ cm}^2 \text{ g}^{-1} & \text{for } T > 1700 \text{ K}. \end{cases} \quad (39)$$

The enhancement factor  $R_e/R$  due to the atmosphere is shown in Fig. 2.

We perform the simulations for embryo formation starting from a monodisperse mass population of planetesimals of mass  $m_0$  and radius  $r_0$  with  $e = 2i = (2m_0/M_*)^{1/3}$  and  $\rho_p = 1 \text{ g cm}^{-3}$  around the central star of mass  $M_\odot$  with a set of eight concentric annuli at 3.2, 4.5, 6.4, 9.0, 13, 18, 25, and 35 AU containing  $\Sigma_{\text{gas}}$  and  $\Sigma_s$  for  $q = 3/2$ . To compute  $Q_D^*$ , we use Equation (5) with  $Q_{0s} = 7.0 \times 10^7 \text{ erg g}^{-1}$ ,  $\beta_s = -0.45$ ,  $Q_{0g} = 2.1 \text{ erg cm}^3 \text{ g}^{-2}$ ,  $\beta_g = 1.19$ , and  $C_{\text{gg}} = 9$  (Benz & Asphaug 1999; Stewart & Leinhardt 2009). We artificially apply the gas surface density evolution in the form

$\Sigma_{\text{gas}} = \Sigma_{\text{gas},0} \exp(-t/T_{\text{gas,dep}})$ , where  $T_{\text{gas,dep}}$  is the gas depletion timescale, which we set to  $T_{\text{gas,dep}} = 10^7$  years. Assuming a constant  $\Sigma_{\text{gas}}$  gives almost the same results for final embryo masses, because we consider time spans  $t \leq T_{\text{gas,dep}}$ .

Fig. 6 shows the embryo-mass evolution at 6.4 AU for  $f = 0.01$ . Runaway growth initially occurs; embryo mass exponentially grows with time during the stage. The runaway-growth timescale is proportional to  $r_0/\Sigma_{s,0}$  (Ormel et al. 2010a,b).

When the embryo masses exceed  $0.001\text{--}0.01M_\oplus$ , oligarchic growth starts. Since massive embryos dynamically excite planetesimals, the reduction of planetesimals due to collisional fragmentation stalls the embryo growth (Kobayashi et al. 2010). For  $\Sigma_0 = 7.1 \text{ g cm}^{-2}$  (MMSN), the fragmentation limits the final mass to about Mars mass ( $\sim 0.1M_\oplus$ ) and the atmosphere is insignificant. Once embryo masses exceed the Mars mass, atmosphere substantially accelerates the embryo growth. For  $\Sigma_0 \geq 21 \text{ g cm}^{-2}$  ( $3\times\text{MMSN}$ ), the atmosphere leads to further embryo growth. Nevertheless, embryos finally attain asymptotic masses.

Results for these simulations are summarised in Fig. 3, where the embryo masses after  $10^7$  years are compared to analytical formulae for final embryo masses. Embryo masses finally reach  $M_a$  inside 5 AU ( $\Sigma_0 = 7.1 \text{ g cm}^{-2}$ ), 10 AU ( $\Sigma_0 = 21 \text{ g cm}^{-2}$ ), and 20 AU ( $\Sigma_0 = 71 \text{ g cm}^{-2}$ ). However, embryos exceed  $M_a$  inside 5 AU for  $\Sigma_0 = 71 \text{ g cm}^{-2}$ . This excess comes from the embryo growth through collisional accretion with bodies drifting from outside, which effect we did not consider in the analysis described in Section 3. To confirm the contribution from drifting bodies, we show the surface density evolution in Fig. 7. For  $\Sigma_0 = 71 \text{ g cm}^{-2}$ , the surface density of solids increases after  $2 \times 10^5$  years. Since the drift timescale shortens inward, bodies from outside cannot raise the surface density unless embryos accrete them. Therefore, the increase in the surface density implies that embryo grows through the accretion of such bodies.

The initial mass  $m_0$  of planetesimals in the simulations depends on their formation process, which is not well understood yet. We perform the embryo growth starting from different  $m_0$  (Figs. 4 and 5). Small planetesimals are relatively easily fragmented due to low  $Q_D^*$  and quickly ground down to the low-mass end of collision cascade.

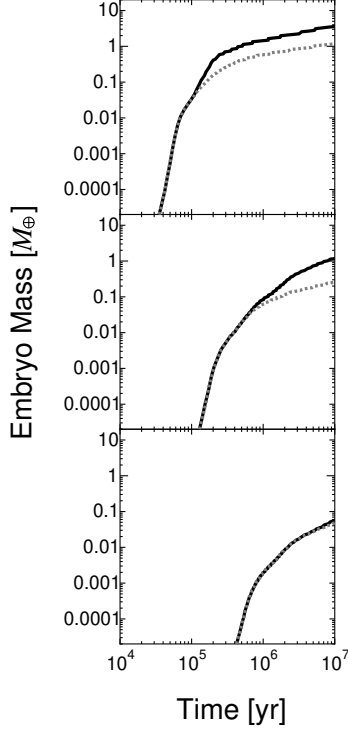


Fig. 6.— Evolution of embryo mass at 6.4 AU with  $m_0 = 4.2 \times 10^{18}$  g ( $r_0 = 10$  km) for  $\Sigma_0 = 71$  g cm $^{-2}$  (10×MMSN; top), 21 g cm $^{-2}$  (3×MMSN; middle), and 7.1 g cm $^{-2}$  (MMSN; bottom). Solid lines show the case with atmosphere and dotted lines represent the result without atmosphere.

The resulting fragments with low  $e$  actively accrete onto embryos. For  $m_0 = 4.2 \times 10^{15}$  g ( $r_0 = 1$  km), embryos can reach a final mass  $M_a$  in a relatively wide region inside 10 AU (MMSN), 20 AU (3×MMSN), and 30 AU (10×MMSN). On the other hand, large initial planetesimals delay the runaway growth of embryos (Ormel et al. 2010a,b) and the following oligarchic growth is also slower than that for small planetesimals because embryos mainly accrete original planetesimals rather than fragments with low  $e$ . For  $r_0 = 100$  km, embryos attain the final masses only inside 4 AU for 3×MMSN and inside 6 AU for 10×MMSN, and embryos cannot reach final masses beyond 2.7 AU in the MMSN disk. In addition, small bodies drifting from outside are effectively captured by embryos and thereby em-

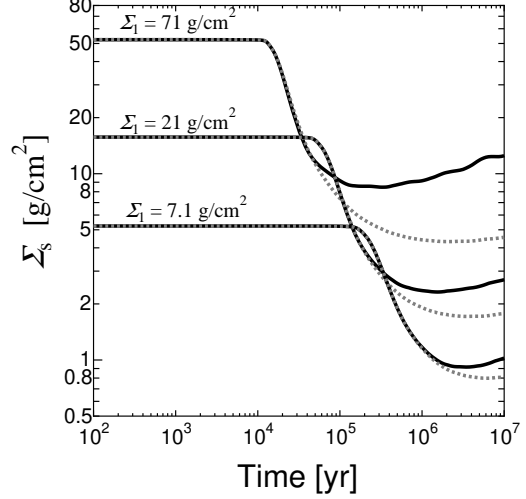


Fig. 7.— The solid surface density evolution at 3.2 AU.

bryos exceed final masses  $M_a$  inside 4 AU for 10×MMSN.

In the case without an atmosphere, initially larger planetesimals can form massive embryos. Since large planetesimals delay embryo growth, embryos made from 100 km-sized initial planetesimals can reach  $10 M_\oplus$  but the location is only inside 3–4 AU even for 10×MMSN (Kobayashi et al. 2010). The case with the atmosphere shows a similar dependence of the final embryo masses on initial planetesimal mass. However, since the atmosphere accelerates embryo growth, embryos larger than  $10 M_\oplus$  are produced inside 8–9 AU of a 10×MMSN disk with 100 km-sized initial planetesimals.

While the final masses of embryos exceed  $10 M_\oplus$  for large initial planetesimals of  $r_0 \gtrsim 100$  km, embryos must reach the critical core mass within the disk lifetime  $T_{\text{gas,dep}}$  to form gas giant planets. The growth timescale is estimated to be  $M/\dot{M}$ , where  $\dot{M}$  is given by Equation (16). The critical distance  $a_c$  inside which embryos can reach  $10 M_\oplus$  is approximately obtained from the condition  $M/\dot{M} < T_{\text{gas,dep}}$  with  $M = 10 M_\oplus$ ,

$$a_c = 9.6 \left( \frac{T_{\text{dep}}}{10^7 \text{ years}} \right)^{20/39} \left( \frac{\Sigma_1}{71 \text{ g cm}^{-2}} \right)^{23/39} \times \left( \frac{r_0}{100 \text{ km}} \right)^{-1/3} \text{ AU}, \quad (40)$$

where we adopt  $m = 100 m_0$  and  $q = 3/2$ . For  $r_0 = 100$  km, the massive disk with  $\Sigma_1 \gtrsim 70 \text{ g cm}^{-2}$  can form such large embryos around 10 AU. In addition, we estimate  $a_c \sim 5$  AU from Equation (40) for a  $10\times\text{MMSN}$  disk with  $r_0 = 10^3$  km. Indeed, the simulation with  $\Sigma_1 = 71 \text{ g cm}^{-2}$  and  $r_0 = 100$  km shows embryos cannot reach  $10 M_\oplus$  beyond 5 AU (see Fig. 8). Therefore, the condition of  $10\times\text{MMSN}$  with  $r_0 \sim 100$  km is necessary to form gas giants around 10 AU.

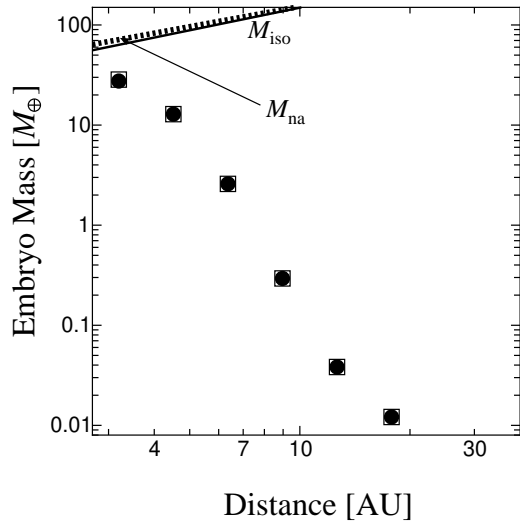


Fig. 8.— Same as Fig. 3, but for  $\Sigma_1 = 71 \text{ g cm}^{-2}$  with  $m_0 = 4.2 \times 10^{24} \text{ g}$  ( $r_0 = 1000$  km). The final mass  $M_a$  with atmosphere is estimated to be larger than  $200 M_\oplus$ .

We also give a constraint on  $f$ . For  $f \lesssim 0.01$ , a final mass is almost independent of  $f$  (see Fig. 9). This is because the gas opacity dominates over the grain opacity (see Equation (39)). For  $f = 1$ , embryos at 3–4 AU become larger due to the capture of bodies drifting from outside, while final embryo masses in the outer disk are similar to the case without atmosphere. The condition of  $f \lesssim 0.01$  is therefore necessary for gas giant formation in the region 5–10 AU and such low  $f$  is acceptable; the depletion factor  $f$  should be much smaller than unity after planetesimal formation. In addition, a low-opacity atmosphere reduces the critical core mass (Mizuno 1980; Ikoma et al. 2000; Hori & Ikoma 2010).

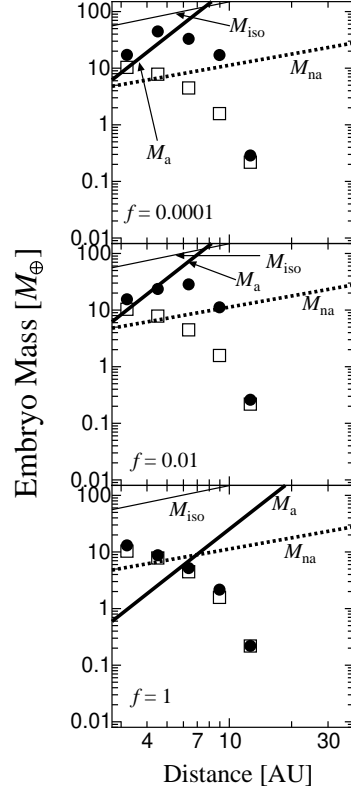


Fig. 9.— The final embryo masses for  $f = 0.0001$  (top), 0.01 (middle) and 1 (bottom), starting from  $10\times\text{MMSN}$  with  $m_0 = 4.2 \times 10^{21} \text{ g}$  ( $r_0 = 100$  km). Lines and symbols are the same as in Fig. 3, but we apply  $\kappa = 1 \text{ cm}^2 \text{ g}^{-1}$  to derive  $M_a$  for  $f = 1$ .

## 5. DISCUSSION

We derived final embryo masses analytically and numerically. They agree with each other quite well in the inner disk where the embryo formation timescale is shorter than the nebula lifetime ( $\sim 10^7$  years). The analytical formula for final masses  $M_a$  implies that initial planetesimal radii should be larger than about  $3 \times 10^3$  km to form embryos with  $10 M_\oplus$  at 5 AU in a MMSN disk. However, the critical distance  $a_c$  inside which embryos reach  $10 M_\oplus$  within  $10^7$  years (Equation (40)) is estimated to be much smaller than 5 AU; a massive disk is likely to form gas giant planets. Embryos inside 5 AU of a  $\sim 10\times\text{MMSN}$  disk exceed final embryo masses  $M_a$  due to the accretion of small bodies drifting from outside. In spite of such further growth, embryos starting from small planetes-

imals cannot reach the critical core mass  $\sim 10 M_{\oplus}$ . In addition, further growth is insignificant beyond 5 AU. The formulae for  $M_a$  and  $a_c$  suggest that initial planetesimals with  $r_0 \simeq 50\text{--}700$  km are necessary for embryos to reach  $10 M_{\oplus}$  at 5 AU in the  $10\times\text{MMSN}$  disk.

Inaba et al. (2003) performed similar simulations incorporating collisional fragmentation and enhancement due to the embryo's atmosphere and showed a planetary core with  $M > 10 M_{\oplus}$  could be produced around 5 AU with  $m_0 = 4.2 \times 10^{18}$  g ( $r_0 = 10$  km) for  $10\times\text{MMSN}$ . In our simulation, embryos cannot reach  $10 M_{\oplus}$  under this condition and larger planetesimals are necessary to form such massive embryos beyond 5 AU. As Kobayashi & Tanaka (2010) discussed, Williams & Wetherill (1994) underestimated the total ejecta mass produced by a single collision for cratering; Inaba et al. adopted the fragmentation model similar to theirs that Wetherill & Stewart (1993) developed (see Fig. 1). Erosive collisions shorten the depletion time of 10 km-sized planetesimals in collision cascade by a factor of 4–5 (Kobayashi & Tanaka 2010) and hence reduce final embryo masses. As seen from Eqs. (24) and (36), final embryo masses  $M_{ca}$ ,  $M_{fa}$  increase with  $Q_D^*$ ; the results of Inaba et al. correspond to embryo masses for higher  $Q_D^*$ . Although we and Inaba et al. applied  $Q_D^*$  provided by Benz & Asphaug (1999), porous bodies with  $r \lesssim 10$  km may have much lower  $Q_D^*$  (e.g., Stewart & Leinhardt 2009; Machii & Nakamura 2011). For initial planetesimals with radii  $\gtrsim 100$  km,  $Q_D^*$  of slightly larger bodies determines final embryo masses and is almost entirely determined by the gravitational binding energy; the uncertainty from their structure would be minor. Therefore, such large planetesimals are possible to produce cores for gas giant planets.

The mechanisms of planetesimal formation are highly debated but, despite intensive effort, remain fairly unknown. The formation through collisional coagulation in which dust smoothly grows to planetesimals with  $r_0 \sim 1$  km face barriers: meter-sized objects should be lost to the central star as a result of gas drag (Weidenschilling 1977; Brauer et al. 2008), and further agglomeration of cm-sized objects upon collision is problematic because of collisional bouncing (Güttler et al. 2010; Zsom et al. 2010). Moreover, the electric repul-

sion may stop growth of smaller objects (Okuzumi 2009). A new scenario that allows one to overcome the barriers has been proposed recently: self-gravity of small particles accumulating in turbulent structures of gaseous disks forms large planetesimals of the order of 100 km (Johansen et al. 2007; Cuzzi et al. 2008). Not only do such large planetesimals produce planetary cores exceeding the critical core mass to form gas giant planets, they may also be consistent with properties of minor bodies in the solar system. Indeed, the initial planetesimals should be larger than 100 km to reproduce the mass distribution of asteroids in the main belt (Morbidelli et al. 2009).

For large planetesimals, a final embryo mass given by  $M_{ca}$  is large enough to start core accretion, while embryo growth is slow. If the radial slope of surface density  $q = 3/2$  like the MMSN model, a massive disk with  $10\times\text{MMSN}$  is necessary for embryos to reach the final mass around 10 AU. However, observations of protoplanetary disks infer their relatively flatter radial distributions over several hundred AU (e.g., Kitamura et al. 2002). In such a disk, dust grains accumulate in an inner disk due to radial drift during their growth, which increases the solid surface density in the inner disk (Brauer et al. 2008). The enhancement of solid surface density accelerates embryo growth and hence embryos may achieve the critical core mass in less massive disks.

To form gas giants via core accretion, rapid gas accretion onto a core with  $\sim 10$  Earth masses must occur prior to gas depletion. However, these cores migrate inward due to their exchange of angular momentum with the surrounding gas (Type I). From linear analysis, the characteristic orbital decay time of Earth-mass cores at several AU in the MMSN model is about 1 Myr (Tanaka et al. 2002). Several processes to delay the timescale of Type I migration have been pointed out, for example, disk surface density transitions (Masset et al. 2006b), intrinsic turbulence (Nelson & Papaloizou 2004), and hydrodynamic feedback (Masset et al. 2006a). There is still uncertainty about this estimate of the migration time. Indeed, the distribution consistent with observations of exoplanets can be reproduced only if the timescale of the type I migration is at least an order of magnitude longer than that derived from the linear analysis (Ida & Lin 2008). We should also investigate the

strength of such migration for the survival of cores of gas giant planets in our future work.

## 6. SUMMARY

In this paper, we investigate the growth of planetary embryos by taking into account, among others, two effects that are of major importance. One of them is collisional fragmentation of planetesimals, which is induced by their gravitational interaction with planetary cores. Another effect is an enhancement of collisional cross section of a growing embryo by a tenuous atmosphere of nebular gas, which becomes substantial when an embryo has reached about a Mars mass.

The main results are summarized as follows.

1. If the atmosphere is not taken into account, collisional fragmentation suppresses planetary embryo growth substantially. As a result, embryos cannot reach the critical core mass of  $\sim 10M_{\oplus}$  needed to trigger rapid gas accretion to form gas giants. The final masses are about Mars mass in a MMSN disk (Kobayashi et al. 2010). Embryo's atmosphere accelerates the embryo growth and may increase the final embryo mass by up to a factor of ten.
2. Planetary embryos attain their final masses asymptotically. We have derived the final mass analytically. The final mass of an embryo is predicted to be the larger of  $M_{\text{ca}}$  and  $M_{\text{fa}}$ , which are given by Eqs. (24) and (36), respectively. These final masses are in good agreement with the results of statistical simulations.
3. Our solution indicates that an initial planetesimal radius  $r_0 \gtrsim 3 \times 10^3$  km is necessary to form a planetary core with  $10 M_{\oplus}$  at 5 AU in a MMSN disk. However, such initially large planetesimals delay embryo growth; a massive disk is required to produce massive cores within a disk lifetime. The analytical solution for the final mass and the embryo formation time show that planetesimals with an initial radius of  $r_0 \simeq 50$ –700 km are likely to produce such a large planetary core within a disk lifetime at 5 AU for  $10\times\text{MMSN}$ .

4. The embryo growth depends on the disk mass, initial planetesimal sizes, and the opacity of atmosphere. We have performed statistical simulations to calculate the final embryo masses over a broad range of parameters. We took the surface density of solids at 1 AU in the range of  $\Sigma_1 = 7.1$ –71 g cm $^{-2}$  ( $1$ – $10\times\text{MMSN}$ ), initial planetesimal radius  $r_0 = 1$ –1000 km, and the grain depletion factor  $f$  in planetary atmosphere between  $f = 10^{-4}$ –1. We found that planetary embryos can exceed  $10M_{\oplus}$  within 8–9 AU for  $10\times\text{MMSN}$ ,  $r_0 = 100$  km, and  $f \leq 0.01$ . Other sets of parameters cannot produce massive cores at 5–10 AU. For example, embryo's mass can reach  $6 M_{\oplus}$  for  $r_0 = 10$  km only inside 4 AU. Therefore, we conclude that a massive disk ( $\sim 10\times\text{MMSN}$ ) with  $r_0 \sim 100$  km and  $f \lesssim 0.01$  is necessary to form gas giant planets around 5–10 AU. This condition for large embryo formation is independent of the material strength and/or structure of bodies, because  $Q_D^*$  of 100 km-sized or larger bodies is largely determined by their self-gravity.

We thank Chris Ormel for helpful discussions and the reviewer, John Chambers, for useful comments on the manuscript.

## REFERENCES

- Adachi, I., Hayashi, C., & Nakazawa, K. 1976, *Progress of Theoretical Physics*, 56, 1756
- Benz, W., & Asphaug, E. 1999, *Icarus*, 142, 5
- Bodenheimer, P., & Pollack, J. B. 1986, *Icarus*, 67, 391
- Bottke, W. F., Durda, D. D., Nesvorný, D., Jedicke, R., Morbidelli, A., Vokrouhlický, D., & Levison, H. F. 2005, *Icarus*, 179, 63
- Brauer, F., Henning, T., & Dullemond, C. P. 2008, *A&A*, 487, L1
- Chambers, J. E. 2006, *ApJ*, 652, L133

- Chambers, J. 2008, *Icarus*, 198, 256
- Cuzzi, J. N., Hogan, R. C., & Shariff, K. 2008, *ApJ*, 687, 1432
- Dohnanyi, J. S. 1969, *J. Geophys. Res.*, 74, 2531
- Fujiwara, A., Kamimoto, G., & Tsukamoto, A. 1977, *Icarus*, 31, 277
- Greenzweig, Y., & Lissauer, J. J. 1992, *Icarus*, 100, 440
- Güttler, C., Blum, J., Zsom, A., Ormel, C. W., & Dullemond, C. P. 2010, *A&A*, 513, A56
- Hayashi, C. 1981, *Progress of Theoretical Physics Supplement*, 70, 35
- Holsapple, K. A. 1993, *Annual Review of Earth and Planetary Sciences*, 21, 333
- Hori, Y., & Ikoma, M. 2010, *ApJ*, 714, 1343
- Housen, K. R., Schmidt, R. M., & Holsapple, K. A. 1991, *Icarus*, 94, 180
- Ida, S., & Lin, D. N. C. 2008, *ApJ*, 673, 487
- Ida, S., & Makino, J. 1993, *Icarus*, 106, 210
- Ida, S., & Nakazawa, K. 1989, *A&A*, 224, 303
- Ikoma, M., Nakazawa, K., & Emori, H. 2000, *ApJ*, 537, 1013
- Inaba, S., & Ikoma, M. 2003, *A&A*, 410, 711
- Inaba, S., Wetherill, G. W., & Ikoma, M. 2003, *Icarus*, 166, 46
- Inaba, S., Tanaka, H., Nakazawa, K., Wetherill, G. W., & Kokubo, E. 2001, *Icarus*, 149, 235
- Inaba, S., Tanaka, H., Ohtsuki, K., & Nakazawa, K. 1999, *Earth, Planets, and Space*, 51, 205
- Johansen, A., Oishi, J. S., Mac Low, M.-M., Klahr, H., Henning, T., & Youdin, A. 2007, *Nature*, 448, 1022
- Kenyon, S. J., & Bromley, B. C. 2004, *AJ*, 127, 513
- Kenyon, S. J., & Bromley, B. C. 2008, *ApJS*, 179, 451
- Kenyon, S. J., & Bromley, B. C. 2009, *ApJ*, 690, L140
- Kitamura, Y., Momose, M., Yokogawa, S., Kawabe, R., Tamura, M., & Ida, S. 2002, *ApJ*, 581, 357
- Kokubo, E., & Ida, S. 1996, *Icarus*, 123, 180
- Kokubo, E., & Ida, S. 1998, *Icarus*, 131, 171
- Kokubo, E., & Ida, S. 2000, *Icarus*, 143, 15
- Kokubo, E., & Ida, S. 2002, *ApJ*, 581, 666
- Kobayashi, H., & Tanaka, H. 2010, *Icarus*, 206, 735
- Kobayashi, H., Tanaka, H., Krivov, A. V., & Inaba, S. 2010, *Icarus*, 209, 836
- Levison, H. F., Thommes, E., & Duncan, M. J. 2010, *AJ*, 139, 1297
- Machii, N., & Nakamura, A. M. 2011, *Icarus*, 211, 885
- Masset, F. S., D’Angelo, G., & Kley, W. 2006, *ApJ*, 652, 730
- Masset, F. S., Morbidelli, A., Crida, A., & Ferreira, J. 2006, *ApJ*, 642, 478
- Mizuno, H. 1980, *Progress of Theoretical Physics*, 64, 544
- Morbidelli, A., Bottke, W. F., Nesvorný, D., & Levison, H. F. 2009, *Icarus*, 204, 558
- Nelson, R. P., & Papaloizou, J. C. B. 2004, *MNRAS*, 350, 849
- Ohtsuki, K. 1999, *Icarus*, 137, 152
- Ohtsuki, K., Stewart, G. R., & Ida, S. 2002, *Icarus*, 155, 436
- Okuzumi, S. 2009, *ApJ*, 698, 1122
- Ormel, C. W., Dullemond, C. P., & Spaans, M. 2010a, *ApJ*, 714, L103
- Ormel, C. W., Dullemond, C. P., & Spaans, M. 2010b, *Icarus*, 210, 507
- Stevenson, D. J. 1982, *Planet. Space Sci.*, 30, 755
- Stewart, G. R., & Ida, S. 2000, *Icarus*, 143, 28



- Stewart, S. T., & Leinhardt, Z. M. 2009, *ApJ*, 691, L133
- Takagi, Y., Mizutani, H., & Kawakami, S.-I. 1984, *Icarus*, 59, 462
- Tanaka, H., Takeuchi, T., & Ward, W. R. 2002, *ApJ*, 565, 1257
- Tanigawa, T., & Ohtsuki, K. 2010, *Icarus*, 205, 658
- Thommes, E. W., Duncan, M. J., & Levison, H. F. 2003, *Icarus*, 161, 431
- Weidenschilling, S. J. 1977, *MNRAS*, 180, 57
- Weidenschilling, S. J. 2005, *Space Sci. Rev.*, 116, 53
- Weidenschilling, S. J. 2008, *Physica Scripta Volume T*, 130, 014021
- Weidenschilling, S. J., Spaute, D., Davis, D. R., Marzari, F., & Ohtsuki, K. 1997, *Icarus*, 128, 429
- Wetherill, G. W., & Stewart, G. R. 1989, *Icarus*, 77, 330
- Wetherill, G. W., & Stewart, G. R. 1993, *Icarus*, 106, 190
- Williams, D. R., & Wetherill, G. W. 1994, *Icarus*, 107, 117
- Zsom, A., Ormel, C. W., Güttler, C., Blum, J., & Dullemond, C. P. 2010, *A&A*, 513, A57